BRITISH STANDARD

BS 7816 :
Part 1 : 1995
IEC 1244-1 :
1993

Determination of long-term radiation ageing in polymers

Part 1. Techniques for monitoring diffusion-limited oxidation

BSI
STANDARDS

Committees responsible for this British Standard

The preparation of this British Standard was entrusted by Technical Committee GEL/15, Insulating material, to Subcommittee GEL/15/2, Endurance tests, upon which the following bodies were represented:

AEA Technology
Adhesive Tape Manufacturers' Association
Association of Manufacturers of Domestic Electrical Appliances
British Cable Makers Confederation
British Plastics Federation
ERA Technology Ltd.
University of Manchester

This British Standard, having been prepared under the direction of the Electrotechnical Sector Board, was published under the authority of the Standards Board and comes into effect on
15 October 1995

The following BSI references relate to the work on this standard:
Committee reference GEL/15/2
Draft announced in *BSI News*, April 1995

ISBN 0 580 24432 6

Amendments issued since publication

Amd. No.	Date	Text affected

Contents

National foreword

This Part of BS 7816 has been prepared by Subcommittee GEL/15/2. It is identical with IEC 1244-1 : 1993 *Determination of long-term radiation on polymers Part 1 Techniques for monitoring diffusion-limited oxidation* published by the International Electrotechnical Commission (IEC).

Compliance with a British Standard does not of itself confer immunity from legal obligations.

INTRODUCTION

It is usually necessary to estimate the anticipated lifetime of a polymeric material in various use environments. For extended lifetimes (years), this often requires the application of accelerated ageing techniques which typically involve the modelling of results obtained at higher-than-ambient environmental stress levels. For many practical applications, air is present during environmental exposures – this usually implies that important oxidation effects underlie the degradation of the material. Unfortunately, exposure of polymers to air during ageing often results in inhomogeneously oxidized samples, a complication which affects attempts both to understand the oxidation process and to extrapolate accelerated exposures to long-term conditions.

The most important inhomogeneous oxidation complication involves diffusion-limited oxidation. The significance of this complication in various environments, including thermal [1]* radiation [2 to 4] and ultraviolet [5] has been recognized for many years. Diffusion-limited oxidation can occur whenever the rate of oxygen consumption in a material is greater than the rate at which oxygen can be resupplied to the interior of the material by diffusion processes from the surrounding air atmosphere. Such instances result in a smooth drop in the oxygen concentration from its equilibrium sorption value at the sample surfaces to a diminished or non-existent value in the sample interior. This will usually lead to a heterogeneity in the oxidation across the material, with equilibrium oxidation (e.g. corresponding to air-saturated conditions) occurring at the sample surfaces, and reduced or little oxidation in the interior.

The importance of the effect will clearly depend upon the material geometry, coupled with the oxygen consumption rate, the oxygen permeability coefficient and the oxygen partial pressure surrounding the sample [5 to 8]. Since the oxygen consumption rate will typically depend upon the environmental stress level (e.g., temperature, radiation dose rate) and both the consumption rate and the permeability coefficient may change as the material degrades [9, 10], the importance of diffusion-limited oxidation will also vary with stress level and degradation. This often implies that the percentage of the sample which is oxidized under accelerated (higher-level) environmental conditions is substantially lower than the percentage oxidized under lower-level application conditions [5 to 7, 10 to 16]. Thus, as has been clear for many years, in order to confidently extrapolate shorter-term accelerated simulations to long-term, air-ageing conditions, a critical requirement is the ability to monitor and quantitatively understand diffusion-limited oxidation effects.

Since a great deal of progress has recently been made in this area, this goal is now realistic. The purpose of this report is to review this area. Clause 2 will describe experimental profiling methods which can be used to monitor diffusion-limited oxidation. Theoretical descriptions of the phenomenon will be briefly given in clause 3. Since the shapes of the theoretical profiles depend upon the oxygen permeability coefficient and the oxygen consumption rate, these quantities must be measured or estimated in order to quantitatively validate the theories. Many experimental methods have been developed for measuring permeability coefficients and a large number of experimental values are

* Figures in square brackets refer to annex B.

available in the literature. Clause 4 will introduce some of the important literature. Experimental methods for estimating oxygen consumption rates will briefly be reviewed in clause 5. Experimental data supporting the theoretical treatments is presented in clause 6. Once confidence in the theoretical treatments exists, the theories can be used either to choose experimental ageing conditions so that diffusion effects are unimportant, or to predict the importance of such effects. If it is impossible to eliminate diffusion effects under air ageing conditions, increasing the oxygen pressure surrounding the sample during ageing may, in certain instances, be used to achieve the desired goal, as outlined in clause 7 on the oxygen overpressure technique.

Part 2 will be published as a separate report and will describe procedures for predicting radiation ageing at low dose-rates.

DETERMINATION OF LONG-TERM RADIATION AGEING IN POLYMERS

Part 1: Techniques for monitoring diffusion-limited oxidation

1 Scope

When oxygen is present during ageing of polymers in various environments including temperature, radiation or ultraviolet, inhomogenous ageing effects caused by diffusion-limited oxidation are often encountered. These effects make it difficult to understand the ageing process and to extrapolate accelerated exposure to long-term conditions. This document reviews experimental techniques to quantitatively monitor these effects and provide theoretical equations to estimate their importance.

2 Profiling techniques to monitor diffusion-limited oxidation

The presence of diffusion-limited oxidation effects implies that various properties related to the amount of oxidation will depend upon spatial location in the material. Thus, any technique which can profile (map) these spatial variations will allow diffusion-limited oxidation to be monitored. Since polymer geometries utilize cross-sections down to a few millimetres or less, and since diffusion-limited oxidation effects are operative over such small dimensions, a useful profiling technique must have a resolution of at least 100 μm. An additional problem related to sensitivity is the observation that severe polymer degradation typically corresponds to less than 1 % of the polymer being oxidized. Thus, a useful profiling technique must have reasonable resolution, good sensitivity to the small chemical changes which occur, wide applicability, and relative ease of operation and analysis. A number of particularly useful techniques are briefly described in this clause.

2.1 *Infra-red profiling techniques*

Because of the ability to provide detailed chemical information on thin film samples, infra-red spectroscopy has been used to monitor diffusion-limited oxidation effects for more than 25 years [17]. Any oxidation-sensitive infra-red peak that can be monitored, either as a function of sample thickness, or as a function of sequentially microtomed slices, will yield information on oxidation heterogeneities. Many of the studies to date have concentrated on the carbonyl region (approx. 1 720 cm^{-1}) of polyolefin materials, such as polyethylene and polypropylene, since infra-red peaks in this region are characterized by high extinction coefficients (high sensitivities) and are usually absent from these materials when unaged. Since the carbonyl region typically represents a superposition of a number of oxidation products (e.g. ketones, aldehydes, esters, acids) of differing extinction coefficients at slightly different wavelengths, simplifying assumptions are often needed to extract semi-quantitative information. In most cases, either the maximum height of the hybrid carbonyl peak or its area is chosen. It should be noted that additives present in commercially formulated materials (e.g. antioxidants, fire retardants) often absorb in the carbonyl region, thereby complicating attempts to use FTIR spectrometry for these materials.

An example of an infra-red profile obtained after microtoming slices off an aged material is shown in figure 1 [18]. A polyolefin material was aged in air for 6 days at 100 °C and the relative oxidation (the absorbance of the carbonyl peak) is plotted versus the depth away from the air-exposed sample surface. The oxidation drops with depth with an approximate exponential dependence; similarly shaped profiles are often observed for heat-aged materials [10, 13, 14].

A second infra-red approach is to create multilayer samples by packing thin films together under mechanical pressure. After ageing, the individual films are separated, then individually analysed. Carbonyl profiles obtained in this fashion for gamma-radiation ageing in air of an unstabilized low-density polyethylene material are shown in figure 2 [19]. The profiles are symmetrical, since both surfaces of the multilayer samples were exposed to air. For these samples, the profiles show a fairly abrupt transition between completely oxidized and unoxidized regions, quite different behaviour from the "exponential" shape observed in figure 1.

Another interesting advance is the use of micro FTIR spectroscopy as a profiling method. Jouan and co-workers [20, 21] pioneered this approach and have used it in photo-oxidation studies to profile the carbonyl peak of a PVC material [20], and product profiles for styrene-butadiene (SBR) and nitrile rubbers [21]. Figure 3 shows product profiles for an SBR film photo-oxidized for 100 h and surrounded on both sides by air [21]. In this case, the drop-off in oxidation away from the surface is similar in shape to the result shown in figure 1.

2.2 *Modulus profiling*

The modulus profiling technique [14, 15] allows one to obtain rapidly and accurately more than 20 quantitative tensile compliance (D) measurements per millimeter of sample cross-section ($1/D$ is closely related to the tensile modulus of the material). This technique is especially useful for elastomers, since the modulus of such materials is very sensitive to scission and cross-linking events and therefore to processing and ageing.

The instrument, which is based on modifications of a thermomechanical analyser, is shown schematically in figure 4. The apparatus measures the indentation of a tiny, paraboloidally-tipped indentor into the sample. A tiny vice (shown in the figure), is used to hold the cross-sectioned samples. After the vice assembly is metallographically polished, indentation measurements under a chosen load are made at selected locations across the cross-sectioned surface. An optical microscope and an X-Y-Z linear positioner are used to quantify the measurement locations. For samples of rectangular cross-section, three samples are held in the vice in a sandwich arrangement with the profiling done across the middle sample. This avoids edge artefacts caused by the high-modulus aluminum plates used as part of the vice. The accuracy (within better than ±10 % of conventional modulus measurements), reproducibility (typically better than ±5 %) and linearity (with load) of the apparatus have been demonstrated on a variety of elastomeric materials [14].

Figures 5 to 7 show modulus profile results for 1,68-mm thick sheets of a commercial Viton®[1] rubber (Parker V747-75), which were gamma-radiation aged in air at 70 °C at three different dose rates. The data are plotted on a normalized thickness basis in which the ordinate, *P*, represents the percentage of the distance from one air-exposed surface of the sample to the opposite air-exposed surface. These profiles have shapes that appear to be intermediate between the "exponential" or "U-shaped" profiles shown in figures 1 and 3 and the "step-shaped" profiles shown in figure 2. For unaged Viton®, the modulus is independent of cross-sectional position and equal to 5,4 MPa; this result is denoted by the horizontal line labelled "unaged". At the highest radiation dose rate of 5,49 kGy/h (figure 5), spectacular heterogeneity, caused by diffusion-limited oxidation, develops with ageing. Oxidative scission occurs near the air-exposed sample surfaces, leading to rapid decreases in modulus. Ageing occurs under essentially anaerobic (inert) conditions in the sample interior, yielding a cross-link-dominated increase in modulus. Since the heterogeneity can be observed after less than 0,04 MGy, which corresponds to relatively moderate changes (10 % to 20 %) in ultimate tensile properties [6, 7, 11], modulus profiling can clearly be sensitive to the earlier stages of ageing. Figure 6 gives results at a six times lower dose rate of 0,9 kGy/h, where diffusion-limited oxidation effects are reduced but still evident. Finally, at 0,14 kGy/h (figure 7), oxidation has been slowed down sufficiently to assure homogeneous oxidation throughout the sample. At high dose rates characteristic of typical accelerated radiation ageing conditions, cross-linking dominates the overall (i.e. macroscopically observed) degradation whereas, under long-term, low dose-rate ageing conditions, scission will predominate. Such results clearly underscore the danger that occurs whenever important diffusion-limited oxidation effects exist for accelerated environments, if the accelerated results are used to make predictions under long-term, low-level environments.

Modulus profiling results [10] for 1,9 mm thick chloroprene rubber samples after ageing in an air-circulating oven at 150 °C and 100 °C are shown in figure 8. Significant and complicated diffusion-limited oxidation effects are evident. At the higher temperature of 150 °C (left plot), diffusion effects exist at the earliest stages of ageing. At the lower temperature of 100 °C (right plot), diffusion effects appear to be less important. In fact, at the early stages of ageing, the oxidation appears to be essentially homogeneous. In the later stages of ageing, however, important diffusion effects become apparent. This phenomenon, of increasingly important diffusion-limited effects with ageing time, is common for elastomers which are thermally aged in air. It is often caused by substantial decreases in oxygen permeation rate which occur as the polymer hardens (modulus increases) with progressive ageing. Other factors contribute [10], for example, the rate of oxygen consumption may increase with ageing time. Sorting out these complicated diffusion-limited effects is clearly necessary if results from accelerated temperature exposures are used to make long-term predictions at much lower temperatures.

[1] Viton® is the trade name of a product supplied by DuPont de Nemours. This information is given for the convenience of users of this Report and does not constitute an endorsement by IEC of the product named. Equivalent products may be used if they can be shown to lead to the same results.

2.3 *Density profiling*

The density profiling technique [13] is based on the use of a density gradient column to obtain the density of successive thin slices cut across a sample. It depends on the fact that oxidation reactions often lead to substantial and easily measurable increases in polymer density. Although a number of methods are available for measuring density, only the density gradient column can yield accurate results on the extremely small samples necessary for achieving the required spatial resolution. To use the density profiling approach, one has to find liquids for the column that are not significantly absorbed by the polymer, since swelling of the material will complicate the interpretation of the data. Since absorption of water by most polyolefins is small, density profiling has been successfully applied to these materials using aqueous salt solutions. Some example density profiling data are plotted in figure 9 for two thicknesses of a commercially formulated EPDM rubber material after radiation ageing in air to 0,32 MGy at 6,65 kGy/h and 70 °C [22]. Since the amount of oxidation is approximately linearly related to the density increase, density changes are plotted as crosses versus cross-sectional position. The vertical span of each cross represents the estimated experimental uncertainty of the measurement, whereas the horizontal span denotes the position and thickness of each slice. The shape of these profiles again lies in the regime that is intermediate between "U-shaped" and "step-shaped". As expected, diffusion-limited oxidation effects become less important as the sample thickness is reduced.

Since density profiling is a much more difficult and time-consuming technique than modulus profiling, the latter technique is generally preferred where applicable, especially for elastomers. However, under certain ageing conditions, elastomers may degrade with an approximate balance between scission and cross-linking events, implying little sensitivity of modulus to ageing. In such instances, density profiling may prove helpful.

2.4 *X-ray microanalysis*

Another recently developed technique for monitoring diffusion-limited oxidation effects involves the use of X-ray microanalysis (XMA) [24]. During oxidation, common products which result on the polymer chain are carboxyl containing groups and peroxide groups. After ageing, a cross-sectional slice of the material is exposed and dipped in a 0,1 N KOH-isopropanol solution in order to convert these groups to potassium-containing species. After conversion, the profile of potassium will therefore represent the oxidation profile for these two oxidation species. The potassium distribution is measured using an electron probe X-ray microanalyser [24].

Figure 10 shows some representative results for an EPDM material which was radiation-aged in air at 1 kGy/h and room temperature. The results indicate that the thickness of the oxidized region is reasonably constant up to doses of at least 330 kGy, implying that the oxygen consumption rate and the oxygen permeability coefficients are reasonably constant up to this dose. Figure 11 shows XMA profiles for this same material after various thermal ageing exposures. It is interesting to note from the 70 °C results that homogeneous oxidation occurs for ageing times up to 4 000 h, but that heterogeneous behaviour becomes significant at longer times. This clearly indicates that the permeability and/or the consumption rate change significantly with ageing time. It is also interesting to note the very different profile shapes observed for the two different ageing environments (radiation versus thermal). In fact the general shapes observed with all of the profiling techniques for thermal ageing exposures (see figures 1, 8 and 11) and for radiation exposures (see figures 2, 5, 6, 9 and 10) are similar.

2.5 *Miscellaneous profiling techniques*

A number of other techniques have shown some promise as profiling tools. For soluble materials, Bowmer and co-workers [25] have used gel permeation chromatography as a method to derive profiles for scission and cross-linking. Another technique sensitive to cross-linking involves the use of nuclear magnetic resonance pulsed field gradient measurements of a material's self-diffusion constant to profile diffusion-limited oxidation effects [26]. Figure 12 shows some results for low-density polyethylene samples radiation aged in air and vacuum. Wilski and co-workers [27, 28] pioneered the use of viscosity profiles to show the importance of diffusion effects for gamma-irradiated polyethylene, polypropylene and PVC. Kuriyama *et al.* [29] obtained gel fraction profiles versus dose rate for gamma-irradiated polyethylene. Chemiluminescence has been successfully applied to gamma-irradiated polypropylene samples by Yoshii *et al.* [30]. Figure 13 shows some of their results. A recent review has been written on experimental methods for monitoring heterogeneous oxidation and covers in more detail many of the above profiling techniques as well as a number of other potentially useful experimental approaches [6].

3 Theoretical treatments of diffusion-limited oxidation

Diffusion-limited oxidation can result whenever oxidation reactions in a material use up oxygen faster than it can be replenished by diffusion effects from the air surrounding the material. Thus, theoretical modelling of diffusion-limited oxidation profiles necessitates combining diffusion equations with expressions for the rate of oxygen consumption, the latter derived from the kinetics appropriate to the oxidation of the material. A particularly useful theoretical treatment of diffusion-limited oxidation for slabs of material of thickness, L, was originally formulated by Cunliffe and Davis [5] using oxidation kinetics which are terminated by bimolecular reactions. More recently, Gillen and Clough [6, 7, 22, 23] showed that very similar theoretical results occur for oxidation kinetics which are terminated by unimolecular reactions. Details of the derivations are given in annex A to this section.

The profiles derived from these theoretical approaches depend upon two parameters, α and β, given by:

$$\alpha = \frac{(C_1 L^2)}{D} \quad (1)$$

$$\beta = C_2 Sp = C_2[O_2]_e \quad (2)$$

where

L is the slab thickness;

C_1 and C_2 are constants involving the kinetic rate constants underlying the chemical degradation,

D and S are the diffusion and solubility parameters for oxygen in the material

p is the oxygen partial pressure of the surrounding atmosphere, and

$[O_2]_e$ denotes the oxygen concentration at the edge of the sample.

Representative theoretical profiles for the normalized oxidation of sheet material exposed on both sides to oxygen are shown in figures 14 to 16 [5 to 7, 23]. P gives the percentage of the distance from one oxygen-exposed surface of the sheet to the opposite oxygen-exposed surface. For small values of β, we find "U-shaped" oxidation profiles; when β is large, the profiles are "step-shaped" with abrupt transitions between oxidized and unoxidized regions of the samples. For intermediate values of β, profile shapes of intermediate character result. Comparison of the theoretical shapes with the experimentally derived profiles shown earlier indicates that, in general, the theories have the flexibility to represent the various shapes of profiles observed.

If experimental data can be used to generate values of the two model parameters α and β, the following theoretical relationship [5], derived in annex A, can be tested:

$$\frac{(R_o L^2)}{pP_{ox}} = \frac{\alpha}{\beta + 1} \quad (3)$$

where

R_o represents the equilibrium oxygen consumption rate, and

P_{ox} is the oxygen permeation rate (equal to D times S) through the material.

We can also use this equation to calculate the critical thickness L_c, below which the integrated oxidation across the sample will be greater than 90 % of a homogeneously oxidized case. We accomplish this by determining the required value of α_c (the α value corresponding to 90 % integrated oxidation) versus β:

$$\frac{(R_o L_c^2)}{pP_{ox}} = \frac{\alpha_c}{\beta + 1} \quad (4)$$

Values of $\alpha_c/(\beta + 1)$ are plotted versus β in figure 17; they vary from ~1,3 at low values of β to ~10 at high values. If we define $C_c = \alpha_c/(\beta + 1)$, equation (4) can be rewritten as:

$$L_c = \left[\frac{C_c \, pP_{ox}}{R_o} \right]^{0,5} \tag{5}$$

If an appropriate value of C_c can be selected, equation (5) allows us to use estimates and/or measurements of R_o and P_{ox} (see clauses 4 and 5 below) to calculate the approximate upper limit on sample thickness if significant diffusion effects are to be avoided. It is clear from the results of figure 17, that even for the currently discussed theory, no single value of C_c can be specified in equation (5). Many researchers [5, 16] have set C_c equal to 8 in order to estimate L_c, a reasonable choice for large values of β ("step-shaped" profiles); others [31] have set it equal to 1, a value clearly appropriate for very small values of β ("U-shaped" profiles). We would like to settle on a single value of this quantity so that, in the absence of profile shape information, we have a simple equation which allows us to estimate the importance of diffusion effects. We select an intermediate value of 4; this gives:

$$L_c = 2 \left[\frac{pP_{ox}}{R_o} \right]^{0,5} \tag{6}$$

an equation which will be utilized and tested in clause 6. Although selecting $C_c = 4$ might seem like an arbitrary choice, it turns out to give reasonable guarantees that samples are homogeneously oxidized, regardless of the profile shape. In the worst case situation of very low values of β, the integrated oxidation across the sample will be greater than 75 % of that appropriate to a homogeneously oxidized sample. Equation (6), therefore, should offer a reasonably general expression for estimating L_c, regardless of the precise details of the underlying oxidation kinetics.

4 Permeation measurements

In order to use equation (6) to estimate the importance of diffusion effects, one needs an estimate of P_{ox}, the oxygen permeability coefficient for the material. Since P_{ox} equals the product of D and S, knowledge of these quantities (the oxygen diffusion and solubility coefficients, respectively) would be equivalent. Fortunately, measurements of these three parameters for oxygen in polymers has been going on for many years, so there is a very large literature describing experimental techniques and data for numerous polymeric materials. There are numerous good reviews and papers, of which a few will be noted [1, 9, 32 to 37]. It is usually possible to obtain an estimate of the oxygen permeability coefficient through the use of a literature search; if literature values are not available, commercially available instruments or analytical service companies can be used to obtain experimental results for a material of interest.

5 Oxygen consumption measurements

Many earlier measurements of the oxygen consumption rate, R_o, for materials were made by monitoring the pressure drop of an oxygen atmosphere surrounding the material during ageing (so-called "oxygen uptake measurements"). This approach is much more difficult to apply in high energy radiation ageing environments. More important, this older technique can easily underestimate the true oxygen uptake, since reaction of the material with oxygen usually leads to the generation of gaseous products, thereby reducing the pressure drop.

More modern approaches use analytical techniques which quantify the amount of oxygen before and after ageing. For instance, a typical approach [38 to 40] involves placing a measured amount of a powdered or thin film polymer in a glass ampoule (known volume) with a break-off seal. The ampoule is filled with a measured amount of oxygen, sealed and then aged in the environment of interest. After ageing, the gases remaining in the ampoule are analysed by gas chromatography. This allows estimates to be made of both the oxygen consumed and of the gases produced from the degradation of the polymer. In carrying out the experiments, it is important to have small enough sample dimensions so that the consumption measurements are being made in the absence of diffusion-limited oxidation! After an experiment is completed, equation (6) can be used, together with an estimate or measurement of the permeability coefficient, P_{ox}, to verify that diffusion effects were absent.

As shown in annex A, even in the absence of diffusion effects, the oxygen consumption rate can depend on the oxygen partial pressure surrounding the sample. This implies that either the average of the initial and final partial pressures in the ampoule should approximate the partial pressure of interest (usually that of air), or that a lack of dependence on partial pressure is verified. For radiation environments, again in the absence of diffusion effects, it should be cautioned that the oxygen consumption rate per Gy of absorbed dose may depend on dose rate [38, 40]. This means that either the lack of dose-rate effects must be verified, or measurements must be made at the dose rate of interest to the ageing or modelling.

6 Comparison of theory with experimental results

We will now quantitatively test [22, 23] the oxidation profile theories summarized earlier in clause 3 (see Annex A for more detailed discussion of the theories). Since the theories assume steady-state conditions, we must choose systems in which R_o and P_{ox} (the oxygen consumption and permeation rates, respectively) are relatively constant with ageing time.

This situation often holds in high energy radiation environments. For example, in gamma-initiated oxidations of commercial elastomers, R_o is often relatively constant up to moderate total radiation doses (0,5 MGy to 1 MGy) [7, 15]. In addition, P_{ox} seldom changes by more than 10 % – 20 % for doses of 0,5 MGy [9]. The EPDM material of figure 9, which was aged to 0,32 MGy at 6,65 kGy/h and 70 °C, met these criteria [22, 23]. Since the density changes plotted in figure 9 are predominantly caused by oxidation, the profile results for the two thicknesses (0,302 cm on left, 0,18 cm on right) were fitted with the theory described in clause 3. The best theoretical fits to the experimental data occur for $\beta = 6$, together with $\alpha = 154{,}5$ (0,302 cm thick sample) and $\alpha = 55$ (0,18 cm thick

sample). These calculated profiles are shown as the solid curves in figure 9. Note that this is a two-parameter fit, since the two values of α must be related by the ratio of the squares of the sample thicknesses, as seen from equation (1). It is clear from the results that the theory does an excellent job of characterizing the profile shapes and their dependence on L. The resulting values of α and β from the fitting procedure yield for the thick sample:

$$\frac{\alpha}{\beta + 1} = 22{,}1 \pm 3 \qquad (7)$$

Separate experiments on the same EPDM material measured the oxygen consumption rate (R_o) as (5,6 ± 0,2) x 10^{-10} moles O_2/Gy/cm^3 and found that oxygen permeation rate at 70 °C was (2,4 ± 0,2) x 10^{-14} mol/(m·Pa·s). These results, coupled with an oxygen partial pressure of 17,6 kPa, give the following for the 0,302 cm thick sample on the left-hand side of equation (3):

$$\frac{R_o L^2}{pP_{ox}} = 22{,}2 \pm 3 \qquad (8)$$

Since this independently calculated result is equal to the result found above in equation (7), the fit is quantitatively consistent with the theoretical relationship given by equation (3).

Now that we have developed some confidence in the theoretical modelling, it is interesting to test equation (6), the theoretical expression for estimating the approximate oxidative penetration distance. For the radiation-aged EPDM sample, equation (6) gives an L_c of 1,27 mm. For the 3,02 mm thick sample (left side of figure 9), this implies an "oxidative penetration depth" reaching ~21 % of the way in from each air-exposed surface; for the 1,8 mm sample (right plot), a depth of ~35 % from each side is predicted. If a sample of thickness equal to ~L_c (1,27 mm) were aged, the full theory (β = 6, α = 27) would predict that the integrated oxidation would be ~90 % of a homogeneously oxidized case. For the Viton® material of figures 5 to 7, R_o is approximately constant and equal to 7,5 x 10^{-10} mole O_2/Gy/cm^3 over the entire dose range of 0 to 1,05 MGy and $P_{ox} \equiv 5{,}0 \times 10^{-15}$ mol/(m·Pa·s) [15]. This leads to an L_c of 0,55 mm at 5,49 kGy/h, which corresponds to a predicted ~17 % penetration of the oxidation in figure 5. At 0,9 kGy/h, L_c increases to 1,36 mm or a predicted 40 % penetration for the data of figure 6. Comparing the results from equation (6) with the experimental profiles, it is clear that approximate relationships such as equation (6) can be very useful for estimating the thickness of sample necessary for eliminating diffusion-limited oxidation effects if estimates or measurements of oxygen permeation and consumption rates are available.

It is also interesting to note that the experimental profiling results for the Viton® material imply that the "oxidative penetration distance" is approximately independent of dose. Since R_o is also found to be independent of dose [15], this implies that P_{ox} must not change dramatically with dose, a result consistent with many other elastomers aged in radiation environments [9].

Finally, it is instructive to apply equation (6) to the early stages of the thermal ageing results for the chloroprene rubber material described in figure 8. At 150 °C, the measured value of R_o for the first day of ageing is $6,7 \times 10^{-3}$ mol/($m^3 \cdot s$) [10]. Although P_{ox} drops dramatically with ageing time, the drop is minor in the first day, so we can estimate that at 150 °C, P_{ox} equals approximately $7,7 \times 10^{-14}$ mol/(m·Pa·s) [10]. This leads to an L_c estimate of 0,89 mm, which corresponds to ~22 % oxidative penetration from each side of the sample, in reasonable agreement with the experimental result after 1 day of ageing. Assuming typical activation energies of 84 kjoule/mol and 42 kjoule/mol, respectively for R_o and P_{ox}, we estimate that L_c equals ~2 mm for the early stages of thermal ageing at 100 °C. This implies initially homogeneous oxidation, in agreement with the experimental results given in figure 8. Later on, at both temperatures, diffusion-limited oxidation becomes more important, primarily due to a significant decrease in P_{ox} caused by the hardening of the material [10].

7 Oxygen overpressure technique

Another interesting approach that can be used to eliminate diffusion-limited oxidation effects is the so-called oxygen overpressure technique, which was pioneered for radiation environments by Seguchi and co-workers [42, 43]. Their apparatus for carrying out such experiments is shown in figure 18 [43]. It consists of a pressure vessel connected to an oxygen source with a pressure regulator and protected with safety equipment, such as safety valves or rupture discs. In radiation environments, the gases evolved from reacting samples must be removed from the vessel for total doses above approximately 0,1 MGy; one method of accomplishing this is to have a continuous leak of the gases (oxygen and product) during irradiation. Because of safety considerations, they recommend that the oxygen pressure be kept below 1 MPa. The pressure vessel is also temperature controlled. Again, because of safety considerations, they recommend that the temperature of the samples during irradiation be kept below 50 °C for pure polymers and 70 °C for formulated polymers (thermal oxidation in pressurized oxygen occurs at lower temperatures than it does in air).

From equation (5), it is clear that increasing the oxygen pressure p, surrounding the sample will result in larger values of L_c, and therefore reductions in diffusion-limited oxidation effects. Since p ~0,02 MPa for air environments, an oxygen overpressure experiment at ~1 MPa will increase L_c by a factor of ~7 times. As discussed above, the value of C_c in equation (5) will depend on the value of β appropriate to the experiment (see figure 17). For radiation ageing under air environments, most evidence (see for example figures 2, 5, 6, 9, 10, 12 and 13) indicates intermediate values of β (e.g. from 3 to 100). Since β is proportional to p (see equation (2)), typical high-pressure oxygen experiments (0,2 MPa to 1 MPa) will increase β by factors of 10 to 50. Thus the β values appropriate at high oxygen pressures should be in the range of 30 to 5 000, implying that C_c in equation (5) would be equal to 9 ± 1, consistent with the value of 8 used by Seguchi and co-workers in their analyses [8, 42]. It should be noted that when β is small to intermediate under air-ageing conditions, raising the oxygen pressure can lead to increases in oxidation at the sample edges, in addition to increasing the oxidative penetration distance into the sample (see annex A). In such instances, increasing the oxygen pressure to eliminate diffusion-limited oxidation effects will eventually result in uniform oxidation throughout the sample, but at a level higher than would occur under air-ageing conditions. Only when evidence exists that the edge oxidation or equivalently the G-factor for oxygen consumption (in radiation environments) is insensitive to oxygen

pressure (e.g. for 0,02 MPa and higher) can the overpressure technique be rigorously used to eliminate diffusion effects. Seguchi and co-workers [38] addressed this issue and confirmed that G-values for oxygen consumption are constant for a number of unstabilized materials over a wide range of oxygen pressures. This implies that the β values for these materials in air are relatively large (e.g. greater than 10).

For radiation-aged materials where chemical dose-rate effects are unimportant (e.g. in the absence of diffusion effects, degradation depends only on the dose, not the dose rate), the oxygen overpressure technique can be used to eliminate diffusion effects at high dose rates and therefore allow lower dose-rate predictions to be made. Figure 19 shows, for example, elongation and tensile strength data for an EPR cable insulation material which was aged at high and low dose rates in air and at a high dose rate in pressurized oxygen. The dose-rate effect observed under the air ageing conditions, caused by the presence of diffusion-limited oxidation at the high dose rate, is eliminated by conducting a high dose-rate experiment in pressurized oxygen.

8 Summary

It should be clear, given the examples shown in this document, that diffusion-limited oxidation effects are commonly observed for polymers aged in air in various environments including thermal, high-energy radiation and ultraviolet. Since these effects can complicate both attempts to understand the oxidative degradation mechanisms and attempts at extrapolating short-term accelerated ageing exposures to long-term ageing conditions, they must be monitored and understood or eliminated/minimized. Recent advances in the development of experimental profiling techniques and in theoretical modelling of the profile shapes now make these goals attainable. A number of the most useful experimental profiling techniques are briefly described in this document; these can be very useful for determining the importance of diffusion effects and monitoring their dependence on experimental ageing conditions. Simplified theoretical models are outlined and the predictions from the models are compared to experiment data. The results of such comparisons lend confidence in the theoretical simulations. Such confidence implies that simple expressions such as equation (6) can be used to estimate, before ageing experiments are begun, the critical combination of sample thickness and accelerating stress level necessary for eliminating diffusion effects. This will help eliminate extraneous and difficult to interpret experimental exposures. Confirmation that diffusion effects are unimportant can then be accomplished using various experimental profiling techniques.

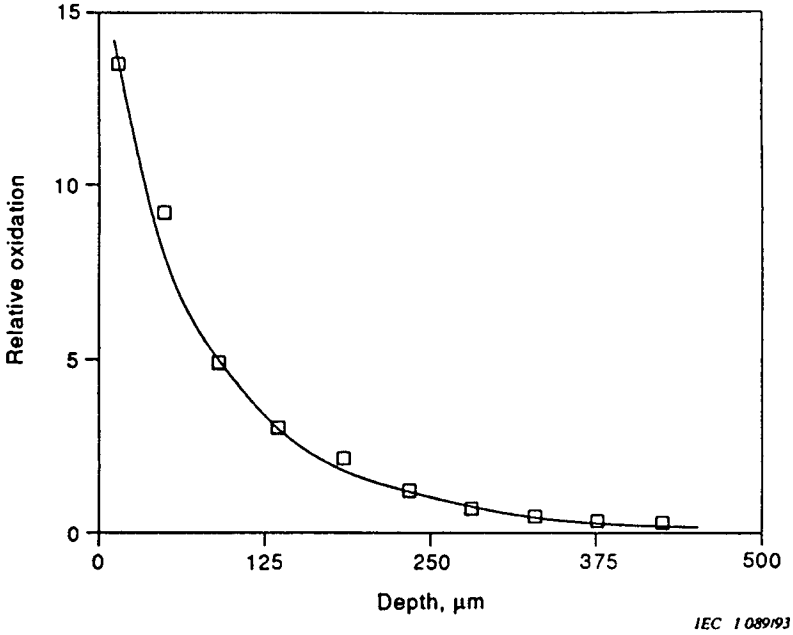

Figure 1 – Relative oxidation as determined from the carbonyl absorbance versus depth away from air-exposed surface of polyolefin material after ageing for 6 days at 100 °C (from [18])

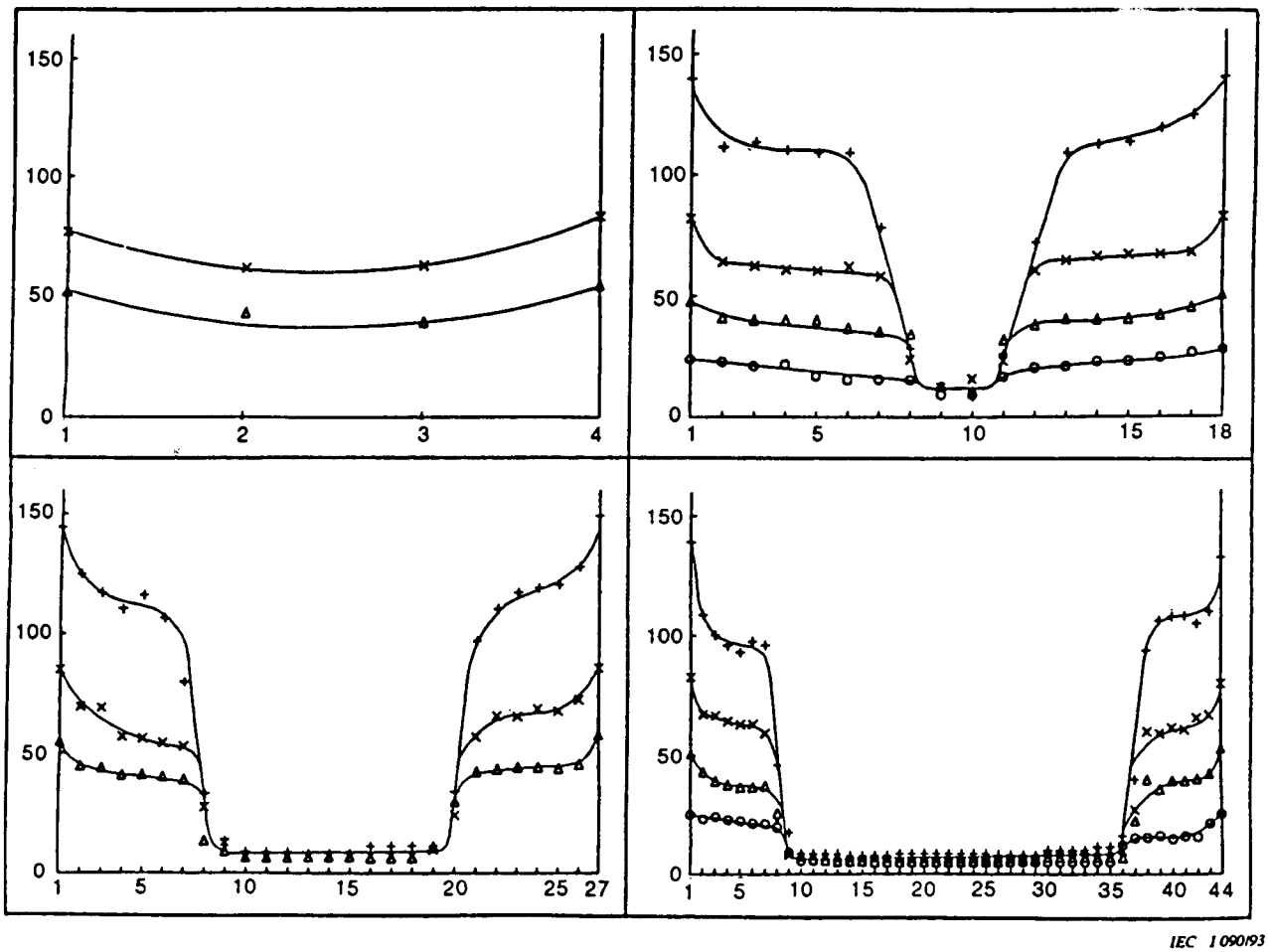

Figure 2 – Depth distribution of carbonyl groups in irradiated (0,69 Gy/s) multilayer samples composed of 4, 18, 27 and 44 films of 22 µm thickness:
○ 0,14; Δ 0,30; × 0,45 and + 0,60 MGy (from [19])

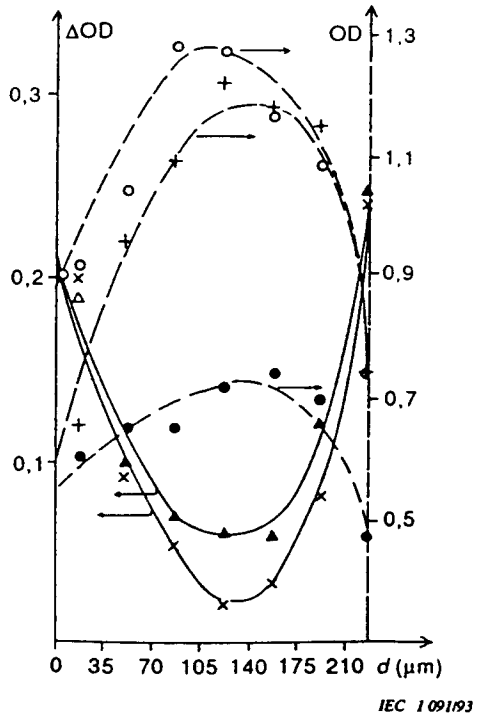

Figure 3 – Micro-FTIR spectrophotometric determination of photoproduct and of residual double-bond profiles in a SBR film photooxidized for 100 h:

▲ carbonyl at 1717 cm^{-1}
× hydroxyl at 3 440 cm^{-1}
○ 1,4-*cis* at 700 cm^{-1}
\+ 1,4-*trans* at 962 cm^{-1}
● 1,2 at 910 cm^{-1}
d represents the width of the slice
(From [21])

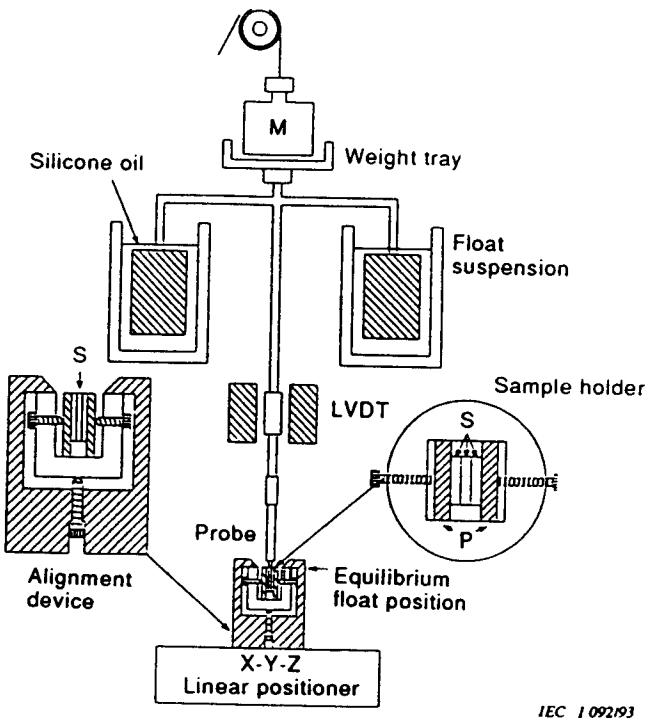

Figure 4 – Schematic diagram of modulus profiling apparatus. The detailed top view of the sample-holder shows three samples labelled with an S held between metal plates P. The detail to the left shows a side view of the sample holder held in the alignment device (from [14, 15])

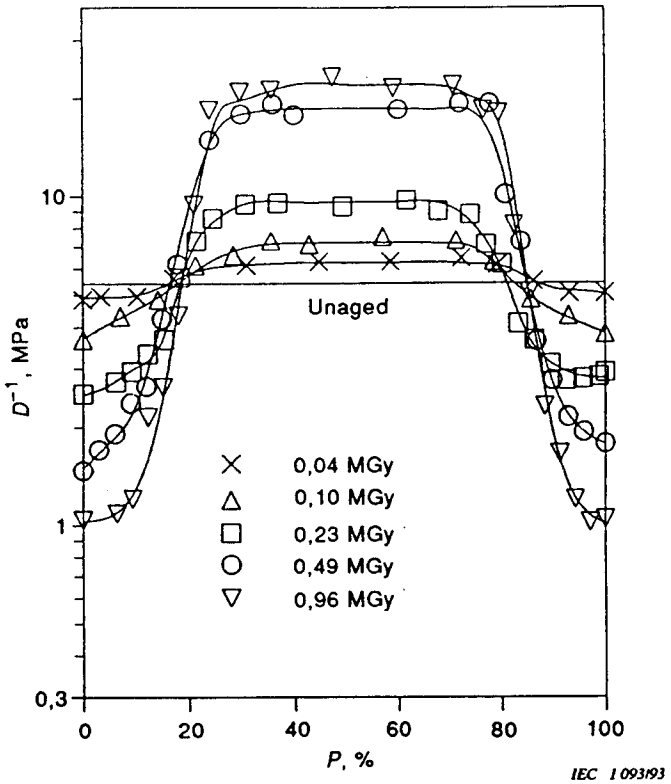

Figure 5 – Modulus profiles of 1,68-mm thick Viton® samples after air ageing at 5,49 kGy/h and 70 °C to the indicated radiation doses (from [15])

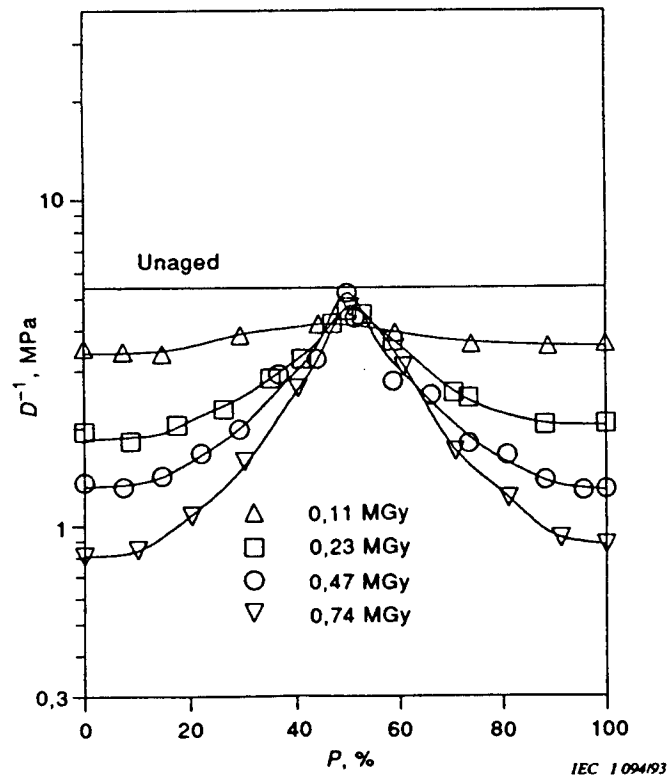

Figure 6 – Modulus profiles of 1,68-mm thick Viton® samples after air ageing at 0,90 kGy/h and 70 °C to the indicated radiation doses (from [15])

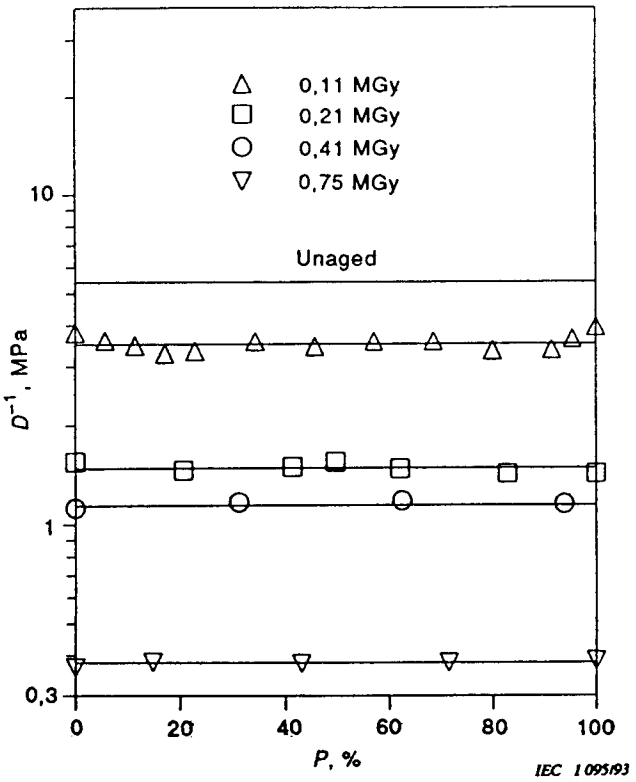

Figure 7 – Modulus profiles of 1,68-mm thick Viton® samples after air ageing at 0,14 kGy/h and 70 °C to the indicated radiation doses (from [15])

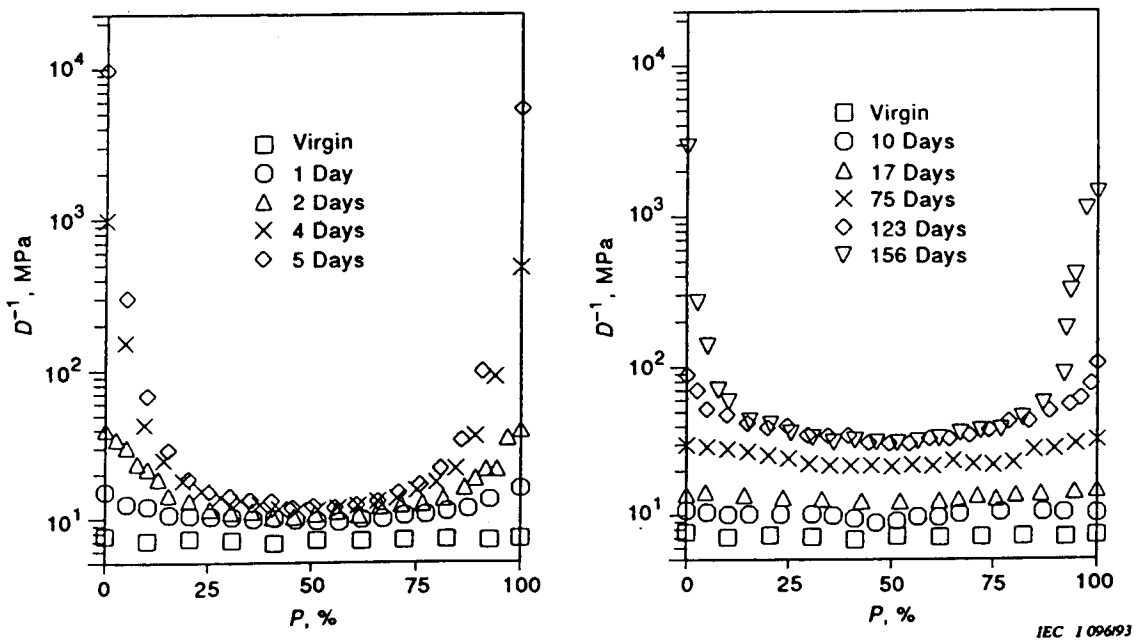

Figure 8 – Modulus profiles of 1,9-mm thick chloroprene rubber samples following elevated temperature exposures in the presence of air at 150 °C, left plot, and 100 °C, right plot (from [10])

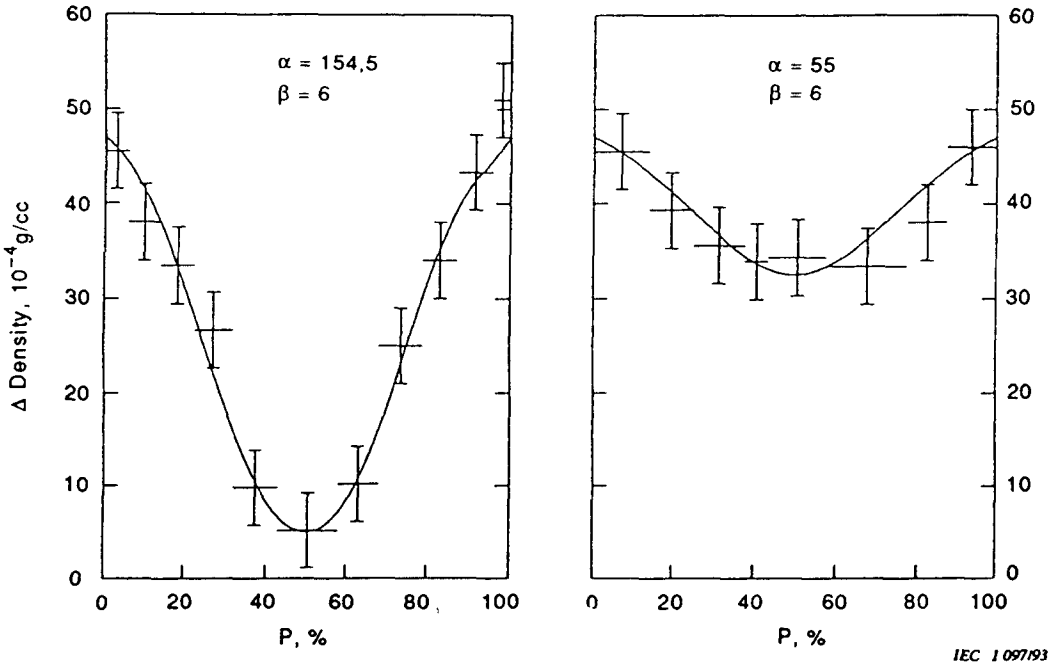

Figure 9 – Experimental density profiles (crosses) for 0,302 cm (left) and 0,18 cm (right) thick EPDM sheets after ageing at 6,65 kGy/h and 70 °C in air. The curves give theoretical fits to the experimental results (from [22, 23])

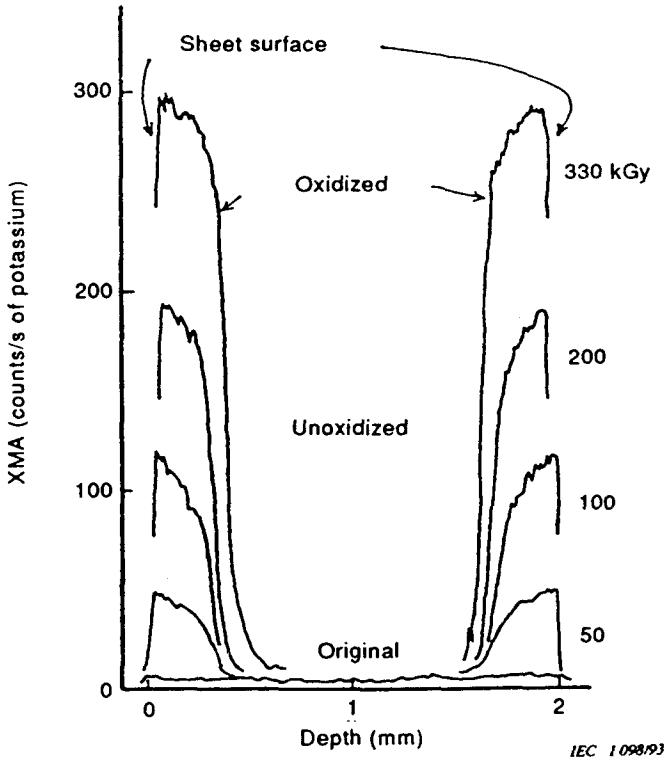

Figure 10 – Effect of total radiation dose on XMA profile for 2-mm thick EPDM sheet irradiated at 1 kGy/h in air (from [24])

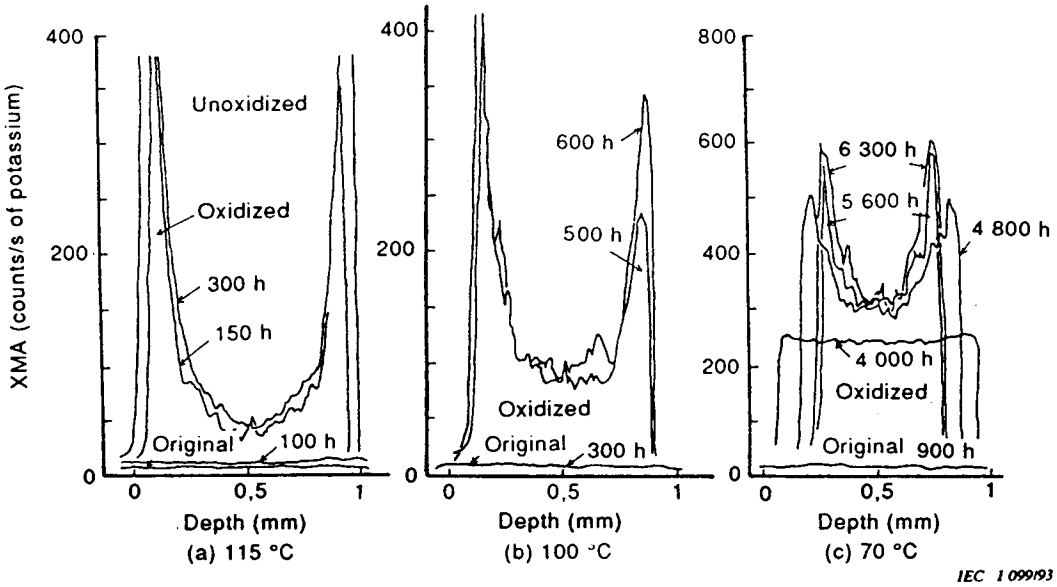

Figure 11 – XMA profiles of 1-mm thick EPDM sheets after thermal ageing in air (from [24])

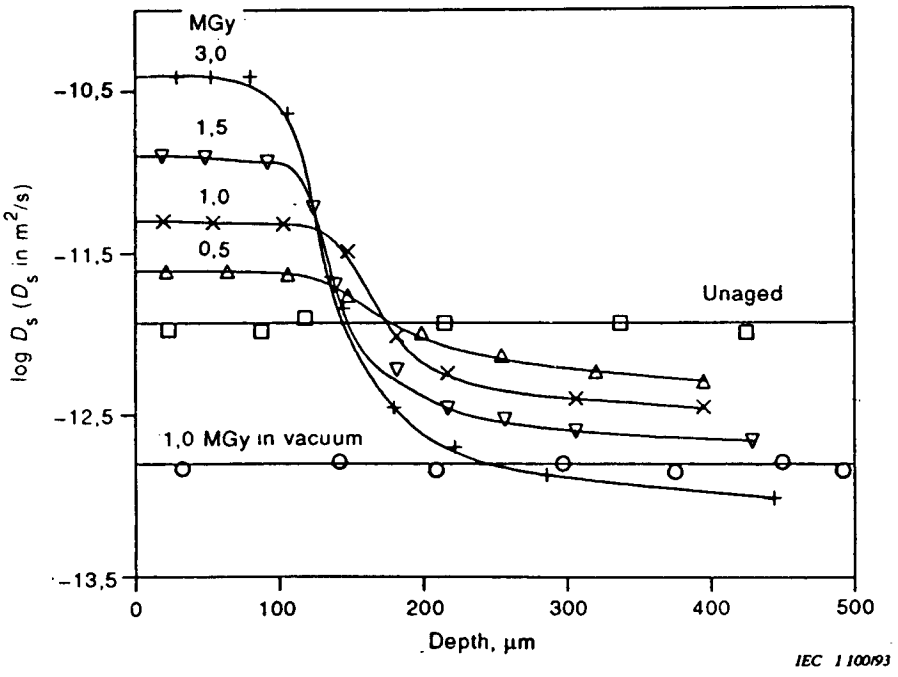

Figure 12 – NMR self-diffusion coefficients versus distance away from sample surface for low-density polyethylene samples after gamma-irradiation in air or vacuum at 0,6 Gy/sec for the indicated total doses (from [26])

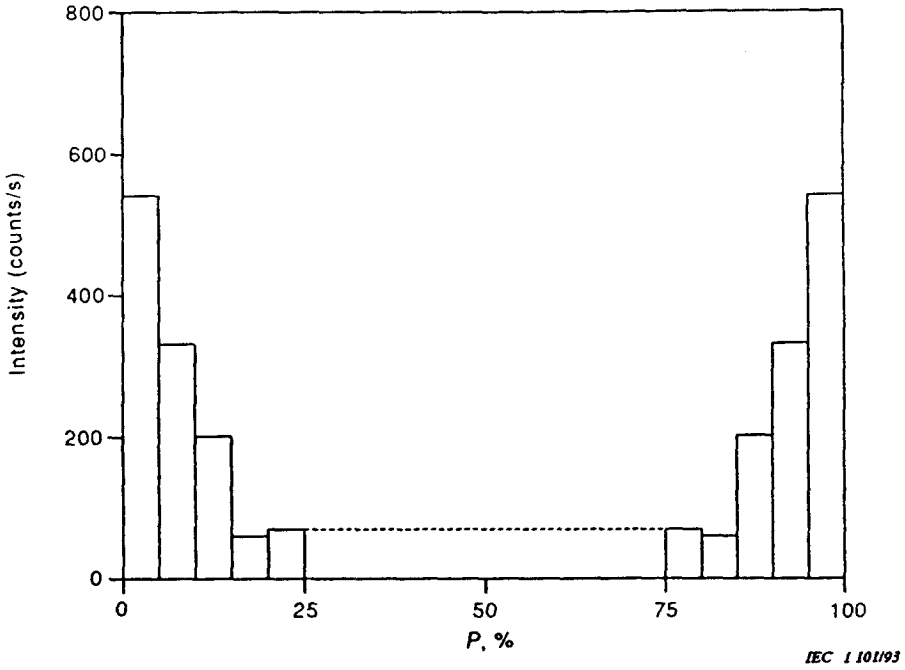

Figure 13 – Chemiluminescence profile for a polypropylene material after gamma-irradiation in air to 0,05 MGy at 2 kGy/h (data from [30])

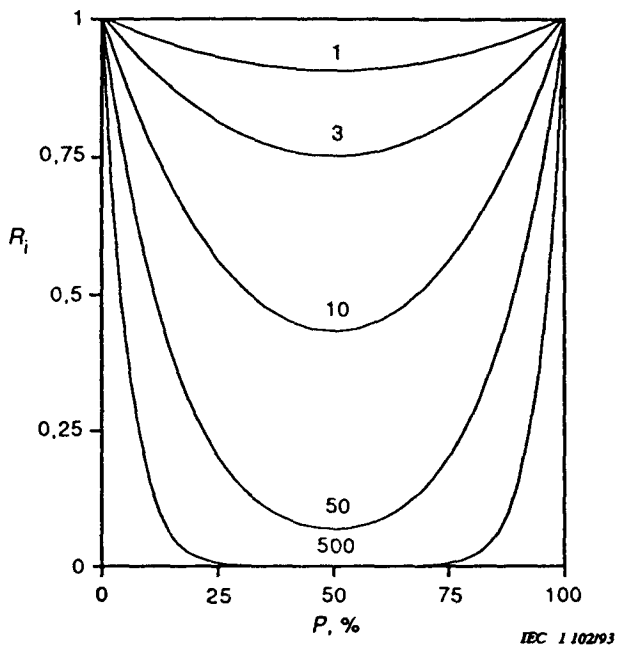

Figure 14 – Theoretical oxidation profiles for various values of α (indicated in figure) with β = 0,1. *P* represents the percentage of the distance from one oxygen-exposed surface of the slab of material to the opposite oxygen-exposed surface (from [7, 23])

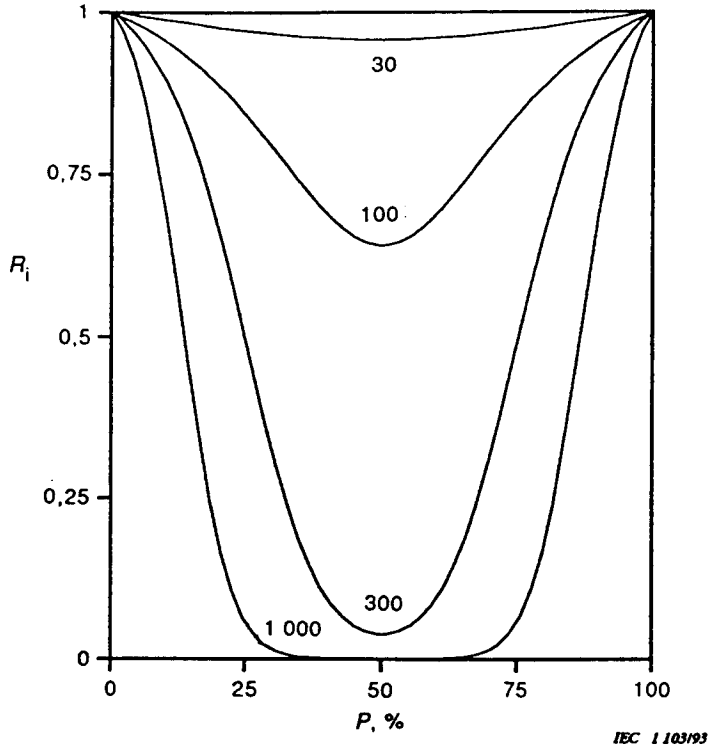

Figure 15 – Identical to figure 14, except that β = 10

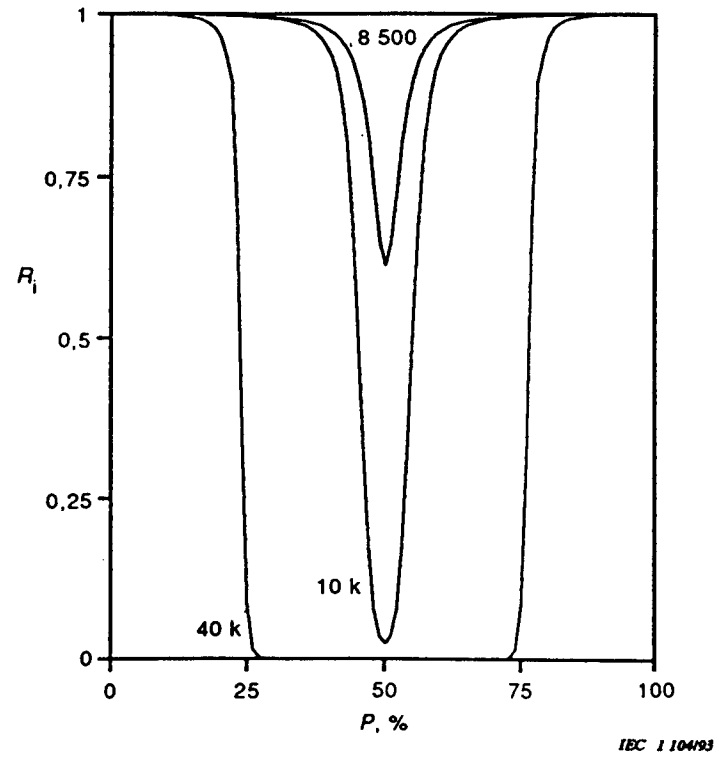

Figure 16 – Identical to figure 14, except that β = 1 000

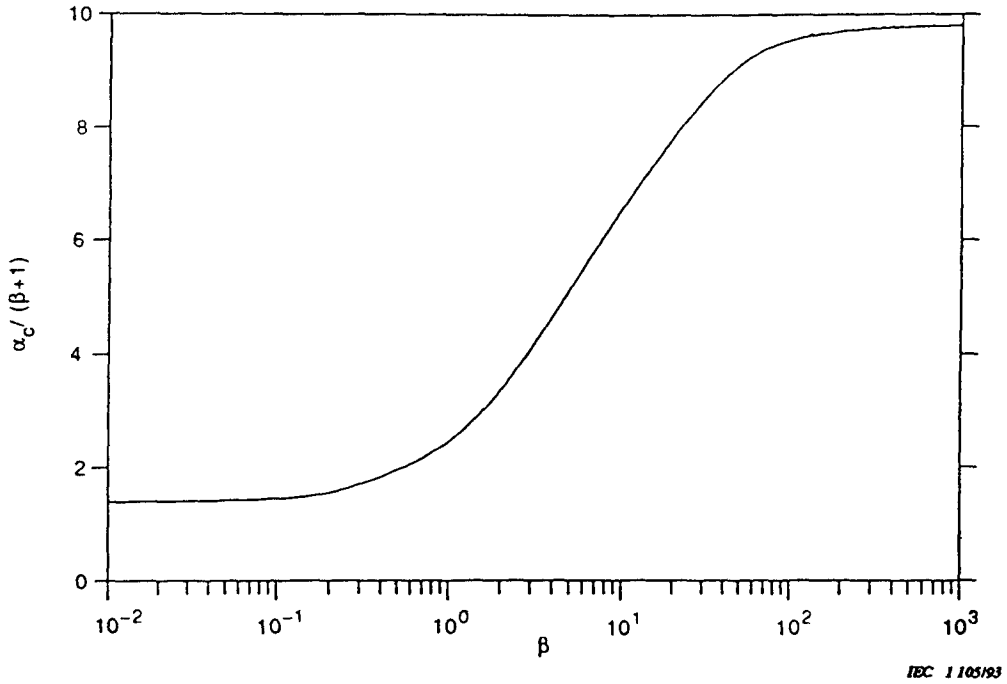

Figure 17 – Plot of $\alpha_c/(\beta + 1)$ versus β, where α_c denotes the value of integrated oxidation corresponding to 90 % (from [7, 23])

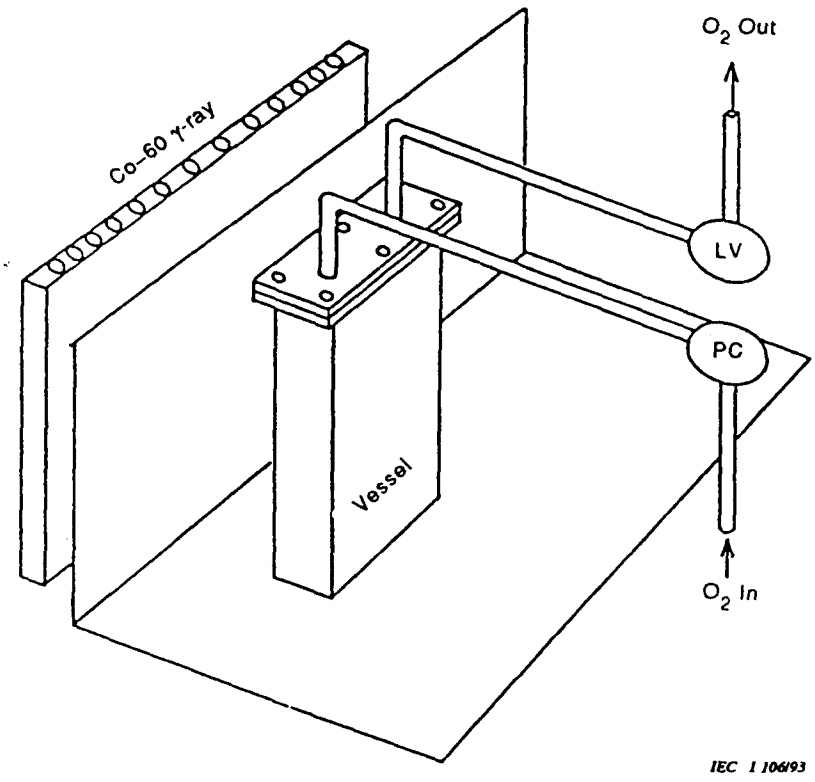

Figure 18 – Apparatus used for irradiation under pressurized oxygen conditions. PC is a pressure regulator, LV is a leak valve (from [43])

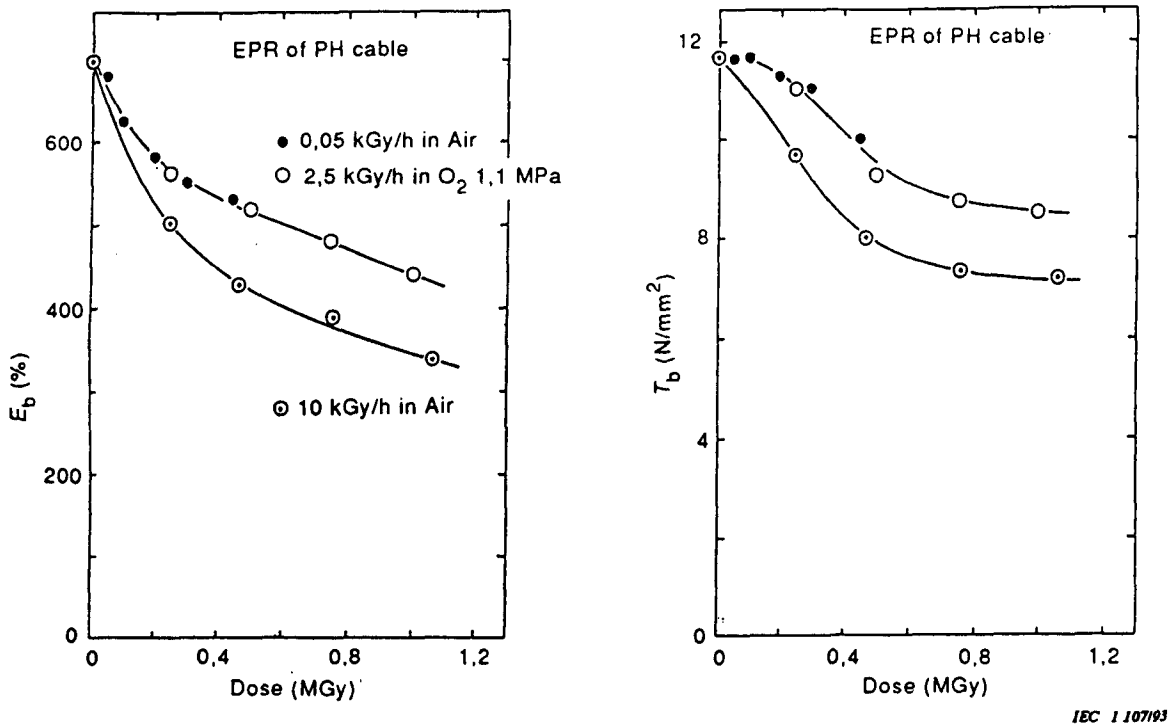

Figure 19 – Tensile elongation (left) and tensile strength (right) data for an EPR material aged at the indicated high and low dose-rates in air and at high dose rate in the pressurized oxygen apparatus of figure 18

Initiation	Polymer	$\xrightarrow{R_i}$	$R\cdot$	(1)
Propagation	$R\cdot + O_2$	$\xrightarrow{k_2}$	$RO_2\cdot$	(2)
	$RO_2\cdot + RH$	$\xrightarrow{k_3'}$	$ROOH + R\cdot$	(3)
Bimolecular termination	$R\cdot + R\cdot$	$\xrightarrow{k_4}$	Products	(4)
	$RO_2\cdot + R\cdot$	$\xrightarrow{k_5}$	Products	(5)
	$RO_2\cdot + RO_2\cdot$	$\xrightarrow{k_6}$	Products + O_2	(6)
Unimolecular termination	$RO_2\cdot$	$\xrightarrow{k_7}$	Products	(7)
	$R\cdot$	$\xrightarrow{k_8}$	Products	(8)
Branching	$ROOH$	$\xrightarrow{k_9}$	$RO\cdot + \cdot OH$	(9)

Figure 20 – Simplified kinetic scheme used to represent the oxidation of polymers (from [44, 45])

Annex A

Derivation of theoretical treatment of diffusion-limited oxidation

The development of theoretical models requires one to combine diffusion relationships with expressions for the oxygen consumption rate in the polymer during ageing. Rigorous derivations of oxygen consumption rates would necessitate detailed knowledge of the complex kinetics underlying the oxidation processes in polymers, an unrealistic goal. In the interest of deriving tractable kinetic expressions, most attempts at modelling oxidation assume that the generic oxidation scheme [44, 45] shown in figure 20 represents a first-order approximation for the oxidation of organic materials, induced by a variety of different stresses (thermal, mechanical, UV light, ionizing radiation, etc.). The main differences occur in the details of the initiation step which first produces the free radical species. It is usually easiest to control the initiation rate in the gamma-initiated case, since R_i is typically independent of ageing time, and linear with the radiation dose rate. In addition, branching reactions, which often enter and complicate the oxidation processes occurring at the high temperatures used for thermal oxidation studies, are often unimportant for lower-temperature, gamma-initiated oxidation. Any growth in importance of branching reactions with ageing time will cause the oxidation rate to increase with time during thermal ageing studies, further complicating attempts to quantitatively model diffusion-limited oxidation. For these reasons, gamma-initiated oxidation appears to represent the simplest possible experimental situation for initial attempts at quantitatively testing diffusion-limited oxidation models. Complications, such as those caused by branching reactions and time-dependent oxidation rates, would then have to be dealt with once confidence existed in the models derived for the simpler experimental situations.

For gamma-initiated oxidations involving moderate temperatures and time periods, we will therefore assume that the chemistry is adequately represented by reactions (1) to (8) in figure 20. The scheme involving the bimolecular termination steps (reactions (1) to (6)), originally derived for the oxidation of organic liquids, has been invoked for many years for explaining the oxidation of polymers. Using a steady-state analysis, and assuming long kinetic chain lengths (many propagation cycles compared to termination reactions), and $k_5^2 = 4\ k_4\ k_6$, the oxygen consumption rate is given by [44]:

$$\frac{dO_2}{dt} = \frac{C_{1b}\,[O_2]}{1 + C_{2b}\,[O_2]} \qquad (9)$$

where

$$C_{1b} = \frac{k_2\ R_i^{0.5}}{(2\ k_4)^{0.5}} \quad \text{and} \quad C_{2b} = \frac{k_6^{0.5}\ k_2}{k_4^{0.5}\ k_3} \qquad (10)$$

and $k_3 = k'_3\,[RH]$.

For many polymeric materials, unimolecular termination reactions are often found to be dominant. For instance, in the presence of sufficient antioxidant, the radical species ($RO_2\cdot$ and $R\cdot$) can terminate in pseudo first-order reactions, yielding an oxidation scheme consisting of reactions (1) to (3) plus (7) and (8). The rate of oxidation is then given by [6, 7, 23]:

$$\frac{dO_2}{dt} = \frac{C_{1u}[O_2]}{1 + C_{2u}[O_2]} \tag{11}$$

where

$$C_{1u} = \frac{k_2 R_i}{k_8} \text{ and } C_{2u} = \frac{k_2 k_7}{k_8 (k_3 + k_7)} \tag{12}$$

It is clear from equations (9) and (11) that the oxygen consumption rates for the unimolecular and bimolecular schemes have identical functional dependencies on the oxygen concentration. However, the constants in the expressions differ, especially in their dependence on the initiation rate, R_i. For the unimolecular case, the oxygen consumption rate depends upon the first power of R_i, whereas it depends on R_i to the one-half power for the bimolecular case. Thus, if reliable data at various well-characterized initiation rates were available, one could distinguish between the two schemes.

By assuming that the oxygen consumption rate and the oxygen permeability coefficient are independent of time, Cunliffe and Davis [5] used the bimolecular kinetic expression for oxygen consumption, and showed that it could be combined with diffusion expressions to derive theoretical oxidation profiles for slabs of material of thickness L. Assuming one dimensional diffusion (L much smaller than the other two slab dimensions), Fickian behaviour and steady-state conditions with the x-coordinate aligned along the thickness direction:

$$D \frac{d^2[O_2(x)]}{dx^2} = -R[O_2(x)] \tag{13}$$

where

$[O_2(x)]$ refers to the concentration of oxygen at the point x,

$R[O_2(x)]$ denotes the rate of removal of oxygen by reaction at x, and

D is the diffusion coefficient for oxygen in the material.

Substituting the kinetic modelling results given in either equation 9 or equation 11 for $R[O_2(x)]$ yields:

$$D \frac{d^2[O_2(x)]}{dx^2} = \frac{C_1[O_2(x)]}{1 + C_2[O_2(x)]} \tag{14}$$

At the surfaces of the sample ($x = 0$ and L), the oxygen concentration must be given by:

$$[O_2(0)] = [O_2(L)] = [O_2]_S = Sp \tag{15}$$

where the surface (equilibrium) oxygen concentration is assumed to follow Henry's law and will therefore be given by the product of S and p, the solubility of oxygen in the polymer and the oxygen partial pressure surrounding the sample, respectively. Another boundary condition occurring at the centre of the sample is:

$$\frac{d\,[O_2\,(L/2)]}{dx} = 0 \qquad (16)$$

Transforming the above with the following reduced variables:

$$X = \frac{x}{L} \quad \text{and} \quad \theta = \frac{[O_2]}{[O_2]_s} \qquad (17)$$

Cunliffe and Davis [5] showed that equation (14) could be written as:

$$\frac{d^2\theta}{dX^2} = \frac{\alpha\theta}{1 + \beta\theta} \qquad (18)$$

where

$$\alpha = \frac{C_1 L^2}{D} \quad \text{and} \quad \beta = C_2 Sp = C_2 [O_2]_s \qquad (19)$$

Although they applied this result to the bimolecular kinetic result (C_1 and C_2 are equal to C_{1b} and C_{2b}, respectively), it is clear that identical results hold for unimolecular kinetics if C_{1u} and C_{2u} are used. The boundary conditions now become $\theta = 1$ at $X = 0$ and $X = 1$, and $d\theta/dX = 0$ at $X = 0{,}5$. Numerical methods lead to a family of solutions for the relative (e.g. normalized to the surface value) oxygen concentration versus spatial position. If θ_i refers to the relative oxygen concentration at point i in the sample, combining either equation (10) or equation (12) with the definitions of α and β leads to the following expression for the oxidation rate at point i:

$$R\,[\theta_i] = \frac{\alpha D \theta_i\,[O_2]_s}{L^2\,(1 + \beta\theta_i)} \qquad (20)$$

Similarly, the oxidation rate at the surface (R_s), which is identical to the equilibrium oxygen consumption rate, is given by:

$$R_s = \frac{\alpha D [O_2]_s}{L^2\,(1 + \beta)} \qquad (21)$$

Thus the relative oxidation at point i is given by:

$$R_i = \frac{R[\theta_i]}{R_s} = \frac{\theta_i\,(1 + \beta)}{1 + \beta\theta_i} \qquad (22)$$

The above analysis can be used to derive theoretical oxidation profiles (plots of R_i versus normalized cross-sectional position) and the corresponding profiles of the relative oxygen concentration (θ_i versus position) [6]. Representative R_i results for three values of β and various values of α are given in figures 14 to 16. By rearranging equation (21) and noting that:

$$D[O_2]_s = pP_{ox} \tag{23}$$

where P_{ox} is the oxygen permeability coefficient through the material, the very useful theoretical relationship given by equation (3) is obtained.

It is also interesting to use the theory to examine the predicted dependence of the oxidation at the surface of the sample on the oxygen partial pressure surrounding the sample. It can be easily seen from either equation (9) or (11), plus equations (1) and (2), that the equilibrium oxygen consumption rate (R_o) or equivalently the oxidation rate at the edge of the material (R_e), is given by:

$$R_o = R_e = \frac{dO_2}{dt} = \frac{C_1 [O_2]_e}{1 + C_2[O_2]_e} = \frac{C_1 Sp}{1 + \beta} \tag{24}$$

Thus, if β_r refers to the value of β at a reference oxygen partial pressure, p_r, the ratio of the edge oxidation rate at an oxygen pressure p, to that under reference conditions, is given by:

$$\frac{R_e (p)}{R_e (p_r)} = \frac{1 + \beta_r}{(p_r/p) + \beta_r} \tag{25}$$

This implies, for instance, that if β is equal to 3 under air-ageing (0,02 MPa) conditions for a given material, increasing the oxygen pressure surrounding the sample to 1 MPa (10 atm) would lead to a 33 % increase in the rate of oxidation at the surface of the sample.

Annexe B/Annex B

Bibliographie/Bibliography

[1] G. J. Amerongen, Rubber Chem. Tech., **37**, 1065 (1964).

[2] H. Matsuo and M. Dole, J. Phys. Chem., **63**, 837 (1959).

[3] A. Charlesby, *Atomic Radiation and Polymers*, Pergamon Press, New York (1960).

[4] A. Chapiro, *Radiation Chemistry of Polymeric Systems*, Interscience Publishers, New York (1962).

[5] A. V. Cunliffe and A. Davis, Polym. Degrad, Stab., **4**, 17 (1982).

[6] K. T. Gillen and R.L. Clough, in *Handbook of Polymer Science and Technology, Vol. 2: Performance Properties of Plastics and Elastomers*, Ch. 6, N. P. Cheremisinoff, Ed., Marcell Dekker, Inc., New York (1989).

[7] K. T. Gillen and R.L. Clough, in *Irradiation Effects on Polymers*, Ch. 4, D. W. Clegg and A. A. Collyer, Eds., Elsevier Applied Science Publishers Ltd., London (1991).

[8] T. Seguchi, S. Hashimoto, W. Kawakami and E. Kuriyama, *Radiation Damage of Polymer Materials. I. Simulation Studies on Distribution of Oxygen Concentration in Polymer Film under Irradiation in Oxygen*, Japan Atomic Energy Research Institute Report, JAERI-M 7315 (1977).

[9] T. Seguchi and Y. Yamamoto, *Diffusion and Solubility of Oxygen in Gamma-Ray Irradiated Polymer Insulation Materials*, Japan Atomic Energy Research Institute Report, JAERI-M 1299 (1986).

[10] R. L. Clough and K. T. Gillen, Polym. Deg. and Stabil., **38**, 47 (1992).

[11] R. L. Clough, K. T. Gillen and C. A. Quintana, J. Polym. Sci., Polym. Chem. Ed., **23**, 359 (1985).

[12] R. L. Clough and K. T. Gillen, in *Polymer Stabilization and Degradation*, ACS Symposium Series No. 280, p. 411, P. P. Klemchuk, Ed., American Chemical Society, Washington, D.C. (1984).

[13] K. T. Gillen, R. L. Clough and N. J. Dhooge, Polymer, **27**, 225 (1986).

[14] K. T. Gillen, R. L. Clough and C. A. Quintana, Polym. Degrad. and Stab., **17**, 31 (1987)

[15] K. T. Gillen and R. L. Clough, Polym. Eng. and Sci., **29**, 29 (1989).

[16] T. Seguchi, S. Hashimoto, K. Arakawa, N. Hayakawa, W. Kawakami and I. Kuriyama, Radiat. Phys. Chem., **17**, 195 (1981).

[17] R. C. Giberson, J. Phys. Chem. **66**, 463 (1962).

[18] J. Y. Moisan, in *Polymer Permeability*, p. 119, J. Comyn, Ed., Elsevier Applied Science Publishers, London (1985).

[19] G. Papet, L. Audouin-Jirackova and J. Verdu, Radiat. Phys. Chem., **33**, 329 (1989).

[20] X. Jouan and J. L. Gardette, Polym. Commun., **28**, 329 (1987).

[21] X. Jouan, C. Adam, D. Fromageot, J. L. Gardette and J. Lemaire, Polym. Degrad. and Stabil., **25**, 247 (1989).

[22] K. T. Gillen and R. L. Clough, Polym. Preprints, **31, No. 2**, 387 (1990).

[23] K. T. Gillen and R. L. Clough in *Radiation Effects on Polymers*, R. L. Clough and S. Shalaby, Eds., ACS Symposium Series, No. 475, American Chemical Society, Washington, D.C. (1991), p. 457.

[24] Y. Morita, T. Yagi and W. Kawakami in *Radiation Effects on Polymers*, R. L. Clough and S. Shalaby, Eds., ACS Symposium Series, No 457, American Chemical Society, Washington, D.C. (1991), p. 485.

[25] T. N. Bowmer, L. K. Cohen, J. H. O'Donnell and D. J. Winzor, J. Appl. Polym. Sci., **24**, 425 (1979).

[26] M. V. Belousova, V. D. Skirda, O. E. Zgadzai, A. I. Maklalov, I. V. Potapova, B. S. Romanov and D. D. Rumyanthev, Acta Polym., **36**, 557 (1985).

[27] H. Wilski, E. Gaube and S. Rosinger, Kerntechnik, **5**, 281 (1963).

[28] H. Wilski, Kunstoffe, **53**, 862 (1963).

[29] I. Kuriyama, N. Hayakawa, Y. Nakase, J. Ogura, H. Yagyu and K. Kasai, IEEE Trans. Electr. Insul., **EI-14**, 272 (1979).

[30] F. Yoshii, T. Sasaki, K. Makuuchi and N. Tamura, J. Appl. Polym. Sci., **31**, 1343 (1986)

[31] N. C. Billingham and P. D. Calvert, in *Developments in Polymer Stabilisation*, Vol. 3, G. Scott, Ed., Applied Science Publishers, Ltd. (1980).

[32] *Polymer Permeability*, J. Comyn, Ed., Elsevier Applied Science, London (1985).

[33] *Engineering Design for Plastics*, E. Baer, Ed., Reinhold Publ. Corp., New York (1964).

[34] R. M. Felder and G. S. Huvard, in *Methods of Experimental Physics*, 16c, pp. 315-377, Academic Press, New York (1980).

[35] V. T. Stannett, Polym. Eng. Sci., **18**, 1129 (1978).

[36] S. T. Hwang, C. S. Choi and K. Kammermeyer, Separ. Sci., **9**, 461 (1974).

[37] S. Pauly in *Polymer Handbook*, 3rd Ed., pp. VI/435-449, J. Brandrup and E. H. Immergut, Eds., John Wiley and Sons, New York (1989).

[38] K. Arakawa, T. Seguchi, Y. Watanabe, N. Hayakawa, J. Polym. Sci., Polym. Chem. Ed., **20**, 2681 (1982).

[39] K. Arakawa, T. Seguchi, N. Hayakawa, S. Muchi, J. Polym. Sci., Polym. Chem. Ed., **21**, 1173 (1983).

[40] K. Arakawa, T. Seguchi, Y, Watanabe, N. Hayakawa, I. Kuriyama, S. Muchi, J. Polym. Sci., Polym. Chem. Ed., **29**, 2123 (1981).

[41] K. Arakawa, T. Seguchi, K. Yoshida, Radiat. Phys. Chem., **27**, 157 (1986).

[42] T. Seguchi, Y. Yamamoto and H. Yagyu, Hitachi Cable Review, **4**, 37 (1985).

[43] T. Seguchi, H. Ito and K. Yoshida, *Design and Construction of Accelerated Ageing Facility for Cables*, Japan Atomic Energy Research Institute Report, JAERI-M 83-089 (1983).

[44] J. L. Bolland, Proc. Roy. Soc., **186**, 218 (1946).

[45] L. Bateman, Quarterly Rev. (London), **8**, 147 (1954).

BS 7816 :
Part 1 : 1995
IEC 1244-1 :
1993

BSI — British Standards Institution

BSI is the independent national body responsible for preparing British Standards. It presents the UK view on standards in Europe and at the international level. It is incorporated by Royal Charter.

Contract requirements

A British Standard does not purport to include all the necessary provisions of a contract. Users of British Standards are responsible for their correct application.

Revisions

British Standards are updated by amendment or revision. Users of British Standards should make sure that they possess the latest amendments or editions.

Any person who finds an inaccuracy or ambiguity while using this British Standard should bring it to the attention of the Quality Manager, BSI without delay so that the matter may be investigated swiftly.

BSI offers members an individual updating service called PLUS which ensures that subscribers automatically receive the latest editions of standards.

Buying standards

Orders for all BSI, international and foreign standards publications should be addressed to Customer Services, Sales Department at Chiswick: Tel: 0181 996 7000; Fax: 0181 996 7001.

In response to orders for international standards, it is BSI policy to supply the BSI implementation of those that have been published as British Standards, unless otherwise requested.

Information on standards

BSI provides a wide range of information on national, European and international standards through its Library, the Standardline Database, the BSI Information Technology Service (BITS) and its Technical Help to Exporters Service. Contact the Information Department at Chiswick: Tel: 0181 996 7111; Fax: 0181 996 7048.

Subscribing members of BSI are kept up to date with standards developments and receive substantial discounts on the purchase price of standards. For details of these and other benefits contact Customer Services, Membership at Chiswick: Tel: 0181 996 7002; Fax: 0181 996 7001.

Copyright

BSI
389 Chiswick High Road
London
W4 4AL

9510—8—0.35k— RTL

ISBN 580 24432 6 Product code 00544015 GEL/15/2